Monthly Notices
of the
ROYAL ASTRONOMICAL SOCIETY

MNRAS **435,** 2268–2273 (2013)
Advance Access publication 2013 August 30

doi:10.1093/mnras/stt1443

ULTRACAM z'-band detection of the secondary eclipse of WASP-12b

D. Föhring,[1]⋆ V. S. Dhillon,[2] Nikku Madhusudhan,[3] T. R. Marsh,[4]
C. M. Copperwheat,[5] S. P. Littlefair[2] and Richard W. Wilson[1]

[1]*Department of Physics, Centre for Advanced Instrumentation, University of Durham, South Road, Durham DH1 3LE, UK*
[2]*Department of Physics and Astronomy, University of Sheffield, Sheffield S3 7RH, UK*
[3]*Department of Physics and Department of Astronomy, Yale University, New Haven, CT 0651, USA*
[4]*Department of Physics, University of Warwick, Coventry CV4 7AL, UK*
[5]*Astrophysics Research Institute, Liverpool John Moores University, Wirral CH41 1LD, UK*

Accepted 2013 August 1. Received 2013 June 21; in original form 2013 April 23

ABSTRACT

We present z'-band secondary eclipse photometry of the highly irradiated hot Jupiter WASP-12b using ULTRACAM on the 4.2 m William Herschel Telescope. We measure a decrease in flux of $\delta = 0.130 \pm 0.013$ per cent during the passage of the planet behind the star, which is significantly deeper than the previous measurement at this wavelength (0.082 ± 0.015 per cent). Our secondary eclipse is best fitted with a mid-eclipse phase, ϕ, that is compatible with a circular orbit $\phi = 0.501 \pm 0.002$, in agreement with previous results. In combination with existing data, our eclipse depth measurement allows us to constrain the characteristics of the planet's atmosphere, which is consistent with a carbon-rich model, with no evidence for a strong thermal inversion. If the difference in eclipse depth reported here compared to that of López-Morales et al. is of physical origin, as opposed to due to systematics, it may be caused by temporal variability in the flux, due to atmospheric dynamics.

Key words: techniques: photometric – stars: individual: WASP-12 – planetary systems.

1 INTRODUCTION

Observations of secondary eclipses provide a powerful means of obtaining information about exoplanetary systems. During a secondary eclipse, as the planet passes behind its host star, a decrease in flux directly corresponding to the planet's emission is observed. Photometric measurements of the secondary eclipse allow us to probe the planet's thermal structure (Deming et al. 2005) and atmospheric composition (Deming et al. 2006), and constrain the orbital eccentricity (Charbonneau et al. 2005), all of which are key in assessing the planet's albedo, energy budget and tidal history. To date, ground-based observations have proved to be invaluable in aiding the atmospheric characterization of transiting hot Jupiters (e.g. de Mooij & Snellen 2009; Sing & López-Morales 2009; Croll et al. 2011; Zhao et al. 2012).

The transiting exoplanet WASP-12b is a large ($1.79R_J$) hot Jupiter on a close (0.0229 au, 1.09 d) orbit around a 6300 K host star (Hebb et al. 2009). It is one of the largest and most intensely irradiated planets currently known, with an equilibrium temperature of $T_{\rm eq} = 2516$ K. The combination of a relatively bright ($1.35\,{\rm M}_{\odot}$, G0V) host star and a large close-in planet with an orientation which enables the viewing of both primary and secondary events makes WASP-12b an ideal system for ground-based follow-up observations.

The overinflated radius of WASP-12b poses a challenge for standard planetary models, which predict an upper limit of $1.2R_J$ for evolved gas giants (Bodenheimer, Laughlin & Lin 2003). Proposed mechanisms for inflation include tidal heating (Ibgui, Burrows & Spiegel 2010), Ohmic dissipation (e.g. Batygin & Stevenson 2010; Huang & Cumming 2012; Perna, Heng & Pont 2012) or strong irradiation (e.g. Enoch, Collier Cameron & Horne 2012). Previous studies of WASP-12b have suggested intense tidal forces, giving it a prolate shape and causing it to lose mass to its host star through tidal stripping (Li et al. 2010). There is also evidence for the presence of a bow shock around the planetary magnetosphere directly in front of the planet (Llama et al. 2011). Previous spectroscopic studies have found that the atmosphere of WASP-12b is lacking a strong thermal inversion and possesses very efficient day–night energy circulation and an extreme overabundance of carbon, both of which are contrary to previous theoretical predictions (Madhusudhan et al. 2011), although this has been recently questioned by newer photometric data (Crossfield et al. 2012).

Theory predicts that the time-scale for circularization of WASP-12b is very short. Initial radial velocity and eclipse measurements have suggested an eccentric orbit (Hebb et al. 2009; López-Morales et al. 2010), but this was later refuted (Campo et al. 2011; Croll et al. 2011; Husnoo et al. 2011). An eccentric orbit would indicate orbital pumping from one or more undetected planets, or a very low tidal dissipation (Li et al. 2010).

Previous observations of emission from the dayside atmosphere of WASP-12b have been reported using the *Spitzer Space Telescope*,

⋆ E-mail: dora.fohring@durham.ac.uk

at 3.6, 4.5, 5.8 and 8 μm (Campo et al. 2011), and from ground-based observations in the *J*, *H*, *Ks* (Croll et al. 2011; Zhao et al. 2012) and z' bands (López-Morales et al. 2010).

In this paper, we present a new, high-precision detection of the z' (9097 Å) emission from the extrasolar planet WASP-12b, and discuss the implications on our understanding of the planet. In Section 2, we describe our observations and data reduction. In Section 3, we detail our light-curve modelling and eclipse detection. In Section 4, we show our method of error estimation, and in Section 5, we compare the emission of the planet to atmospheric models. Finally, we discuss our results and provide conclusions in Sections 6 and 7.

2 OBSERVATIONS AND DATA REDUCTION

The secondary eclipse of WASP-12b was observed on 2010 January 5–6 at the 4.2 m William Herschel Telescope on La Palma using ULTRACAM (Dhillon et al. 2007). A total of 3592 observations were made in the SDSS u', g' and z' filters between 22:54 UT and 05:30 UT during excellent transparency conditions. We obtained 3.05 h of out-of-eclipse data and 2.70 h of in-eclipse data at airmasses between 1.000 and 2.319. The telescope was defocussed to give a stellar full width at half-maximum of ∼5 arcsec, enabling longer integration times without saturation, and reducing the effects of pixel sensitivity variations across the stellar profile (see Southworth et al. 2009). An exposure time of 5.6 s was used throughout the run, with a dead time between each exposure of 25 ms. Each frame was time stamped to sub-millisecond accuracy using a dedicated GPS system (Dhillon et al. 2007).

The data were corrected for bias and flat-fielded using the ULTRACAM pipeline software.[1] The effect of correcting the fringing that was apparent in the z' filter was investigated in detail using a fringe frame constructed from night-sky frames; it was found that this correction did not produce a marked difference in the light curves and so was not employed in the final reduction.

We performed aperture photometry on the target and the brightest nine comparison stars in the 5 arcmin × 5 arcmin field using aperture sizes of radii 15–50 pixels (4.5–15 arcsec). The best aperture was the one that produced the most stable photometry with the lowest variance in segments of the out-of-eclipse and mid-eclipse regions of the resulting light curve, and was found using a golden section search (Kiefer 1935). For our data, this resulted in an aperture of 42 pixels. The centres of each star were determined by fitting a Moffat profile (Moffat 1969) to the point spread function of each star. We decided to add an extra aperture on our target to include a background star, ∼10 arcsec from WASP-12 and partially overlapping our optimum aperture, as this improved the variance. The implications of this are discussed in Section 4. We found that the size of the sky annulus did not have a significant effect on the photometry, and kept it constant with an inner radius of 60 pixels and outer radius of 90 pixels. The sky background level was determined using a clipped mean method, with fainter background stars masked out from the sky annuli.

We produced a single light curve by combining individual differential light curves that were produced from the three brightest comparison stars in the field, which had similar flux levels to the target in the z' band. The individual light curves were weighted based on the inverse chi-square of a straight-line fit to their out-of-eclipse and mid-eclipse sections. The scatter per point on this final light curve was measured as 0.14 mmag, or 0.013 per cent.

In our data, the total drift in the pointing of WASP-12 on the CCDs was 14 pixels in x and 24 pixels in y. We tested our data for systematic correlations with x and y positions of the target on the detector, seeing, sky brightness variations and telescope parallactic angle. This was done by fitting linear correlations between each parameter and the out-of-eclipse portions of the light curve. We did not find any correlations. We discarded the latter 1.36 h of the out-of-eclipse data precisely at the onset of sudden transparency variations, as they caused the scatter per point to increase by up to a factor of 100. This left a total of 2740 observations between 22:54 UT and 04:08 UT, covering phases 0.426 and 0.594 based on the ephemeris of Hebb et al. (2009), and airmasses between 1.000 and 1.477.

3 ECLIPSE MODELLING

To establish the presence of an eclipse, we modelled the light curve using the technique outlined by Sackett (1999) without limb darkening. The input parameters of the model include the radii of the star and planet, the semimajor axis, the orbital inclination and the ephemeris, as given by Hebb et al. (2009). We also attempted to use the system parameters determined by Chan et al. (2011), but found that the duration of the eclipse matches that found by Hebb et al. (2009) more closely and yields a lower chi-squared fit.

The best-fitting model was found by using a downhill simplex χ^2 minimization routine (Press et al. 2007), with the eclipse depth, δ, the phase of mid-eclipse, ϕ, and two background terms, c_1 and c_2, as free parameters. The two background terms allow the out-of-eclipse differential flux, B, to be fitted by an equation of the form: $B = c_1 + c_2 X$, where X is the airmass. The best-fitting model, shown in Fig. 1, is an eclipse with a depth of $\delta = 0.130$ per cent, centred at an orbital phase $\phi = 0.501$. The reduced χ^2 of the fit is 1.083.

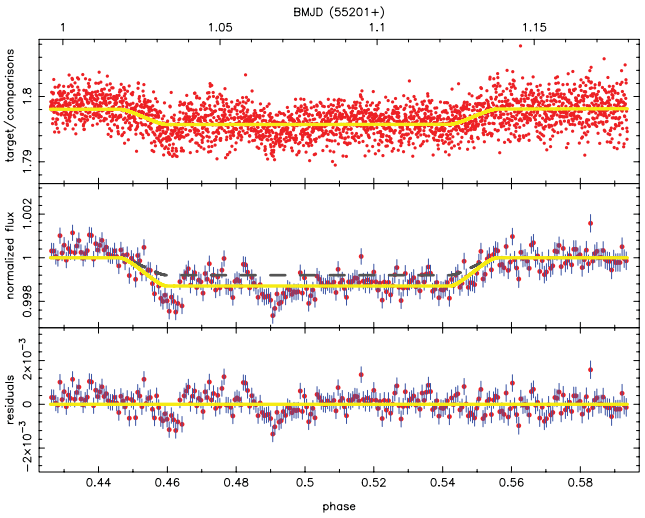

Figure 1. Secondary eclipse of WASP-12b observed in the z' band. The top panel shows the unbinned raw light curve, with the best-fitting secondary eclipse model (including background) overplotted in yellow (see Section 3). The middle panel shows the background-subtracted and normalized light curve with the data binned into groups of 10 data points, corresponding to 1 min, again with the best-fitting model overplotted. The grey dashed line shows a depth of 0.082 per cent as found by López-Morales et al. (2010). The bottom panel shows the residuals after subtraction of the best-fitting model from the data shown in the middle panel.

[1] http://deneb.astro.warwick.ac.uk/phsaap/software/ultracam/html/index.html

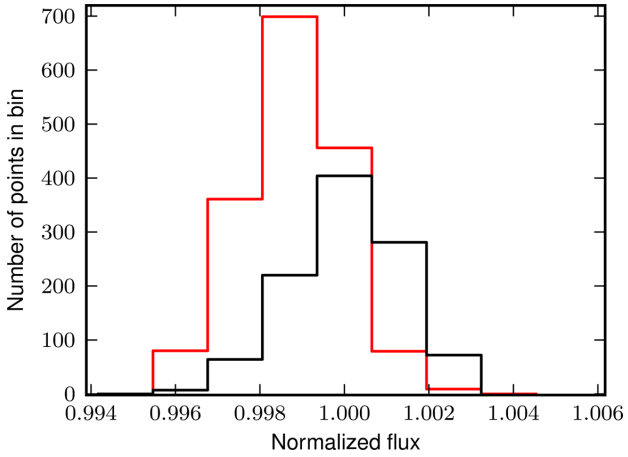

Figure 2. Histograms of the in-eclipse (red line) and out-of-eclipse portions of the normalized WASP-12b light curve. The width of each bin is 0.13 per cent, the same as the eclipse depth.

We also searched for evidence of a secondary eclipse in the g' and u' bands and found our results consistent with no detection in either.

We performed two tests to confirm the eclipse detection, in a manner similar to previously reported eclipse results (Deming et al. 2005; Rogers et al. 2009; López-Morales et al. 2010). In the first test, we averaged all of the fully in-eclipse data points from the background-corrected light curve and repeated this for all of the out-of-eclipse points. The difference between the two measurements gives an eclipse depth of 0.135 ± 0.005 per cent, where the error is calculated from the scatter on our in-eclipse and out-of-eclipse data points.

In the second test, we generated histograms of the in-eclipse and out-of-eclipse portions of the normalized light curve, and set the bin width equal to the measured eclipse depth. The result, shown in Fig. 2, illustrates how the flux distribution of in-eclipse points is shifted by one bin, as expected, with respect to the out-of-eclipse flux distribution centred on 1.0.

4 ERROR ESTIMATION

To compute the error in the eclipse depth and to determine the extent of systematics, we employ the binning technique described by Pont, Zucker & Queloz (2006). Using this method, the uncertainty on the eclipse depth, $\sigma(N)$, is approximated as the error on the mean of the in-eclipse flux. In the absence of correlated noise, $\sigma(N) = \sigma_w/\sqrt{N}$, where N is the number of points in a given interval, here the eclipse, and σ_w is the measurement uncertainty, which can be obtained from the uncorrelated root-mean-square (rms) scatter per out-of-eclipse data points. When taking into account the covariance of the data on the time-scales of the eclipse, the error on the eclipse depth can be shown to be well modelled by the relation $\sigma(N)^2 = \sigma_w^2/N + \sigma_r^2$, where σ_r is the systematic (red) noise component. The uncertainty $\sigma(N)$ can be estimated from the data by binning the out-of-eclipse points in time in intervals of N points: the rms scatter of the binned residuals will follow an $N^{-1/2}$ relation in the absence of red noise; otherwise, they will be fitted by $\sigma^2(N) = \sigma_w^2/N + \sigma_r^2$. Binning our data up to the time-scales of the ingress and egress duration of 21 min ($N = 220$), as shown in Fig. 3, we find $\sigma(220) \simeq \sigma_r = 0.013$ per cent.

We investigated the extent to which uncertainties in the system parameters affect our eclipse depth and mid-eclipse results. By varying the inclination, planet-to-star radius ratio and semimajor axis of the system by 1σ from the reported values in Hebb et al. (2009), the measured eclipse depth changed by a maximum of 3.59 per cent or 0.28σ, while the mid-eclipse phase changed by 0.0004 per cent.

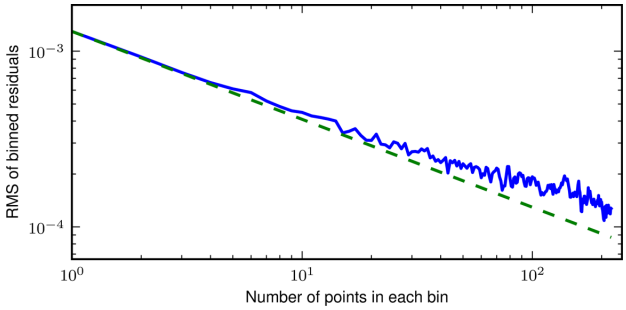

Figure 3. The rms scatter of our out-of-eclipse photometry (solid line), plotted as a function of the light-curve binning factor. The dashed line displays the expectation for Gaussian noise.

We calculated two independent values of the errors in the eclipse depth and the phase of mid-eclipse using the prayer-bead (Gillon et al. 2009) and bootstrapping (Press et al. 2007) techniques in order to estimate the error on the mid-eclipse phase. These provided estimates of $\phi = 0.501 \pm 0.002$, $\delta = 0.130 \pm 0.002$ per cent and $\phi = 0.5014 \pm 0.0004$, $\delta = 0.1298 \pm 0.0003$ per cent, respectively. Taking the final values for eclipse depth and mid-eclipse phase from the downhill simplex results and the errors from the most conservative estimate out of the Pont et al. (2006) method, prayer-bead and bootstrap yielded the final result for the phase of mid-eclipse and the eclipse depth as $\phi = 0.501 \pm 0.002$ and $\delta = 0.130 \pm 0.013$ per cent.

It is necessary to discuss the implication of including additional background stars in our aperture photometry, as discussed in Section 2. In their paper, Crossfield et al. (2012) calculate that including an unresolved M dwarf star with a 1 arcsec separation from WASP-12 (Bergfors et al. 2011, 2013) in the photometry aperture dilutes the measured eclipse depth by 3.97 per cent in the z' band. Accounting for this star in our measurement results in an eclipse depth of 0.135 per cent. A second faint background star was also included in our aperture, which we have determined from our in-focus images contributes an additional dilution of 0.9 per cent. This gives a total corrected eclipse depth of 0.136 per cent, which is within our error of ± 0.013 per cent.

5 COMPARISON WITH ATMOSPHERIC MODELS

We used our z'-band planet–star flux contrast, together with previously published data, to constrain the atmospheric properties of WASP-12b. We modelled the dayside atmosphere of WASP-12b using the approach followed in Madhusudhan (2012). The model, first developed in Madhusudhan & Seager (2009), considers 1D line-by-line radiative transfer in a plane-parallel atmosphere, with constraints of local thermodynamic equilibrium, hydrostatic equilibrium and global energy balance, and includes the major molecular and collision-induced opacity sources expected in hydrogen-rich atmospheres. The temperature profile and molecular abundances constitute 12 free parameters of the model: six parameters for the temperature profile and six for the molecular abundances of H_2O, CO, CH_4, CO_2, C_2H_2 and HCN. Given the data, we explored the space of temperature profiles and composition, both oxygen rich and carbon rich (Madhusudhan 2012), using a Markov chain Monte

Carlo optimization algorithm (Madhusudhan et al. 2011) to find model fits to data.

We assumed that all the z'-band flux arose from thermal emission, in accordance with López-Morales & Seager (2007), who showed that reflected light emission contributes 10—20 times less than thermal emission for very hot Jupiters, such as WASP-12b. We fitted models of WASP-12b to our observed z'-band flux together with existing photometric data in the *J*, *H* and *K* bands (Croll et al. 2011), four channels of *Spitzer* Infrared Array Camera (IRAC) photometry (Campo et al. 2011; Cowan et al. 2012) and a narrow-band photometric observation at 2.3 μm (Crossfield et al. 2012). For the two IRAC data points at 3.6 and 4.5 μm, we adopt the values from Cowan et al. (2012), which have more conservative error bars. For the 4.5 μm point, for which two values have been reported by Cowan et al. (2012), we choose the value that is consistent with the value reported by Campo et al. (2011). For all the previously published data, we use the revised values from Crossfield et al. (2012) which have been corrected for the presence of a stellar companion. A model fit to all the data is shown in Fig. 4. We found that a carbon-rich model (with C/O ≥ 1) with a weak thermal inversion in its dayside atmosphere provides the best fit to all the present data, in agreement with Madhusudhan et al. (2011) and Madhusudhan (2012). The model spectrum shown in Fig. 4, of an atmosphere that is carbon rich and has no thermal inversion, provides a good fit to the data and has a χ^2 of 22.9. We also explored models with isothermal temperature profiles as suggested by Crossfield et al. (2012), and found that the best-fitting isothermal model (with one free parameter) has a temperature of 3135 K and a χ^2 of 48.8. To account for the different number of free parameters, we compared the models using the Bayesian information criterion (Schwarz 1978), defined as $\mathrm{BIC} = \hat{\mathrm{E}}\chi^2 + N_{\mathrm{par}} \times \ln(N_{\mathrm{dat}})$, where N_{par} is the number of free parameters and N_{dat} is the number of data. The BIC for the carbon-rich model was 49.3, lower than the value of 51.0 obtained for the isothermal model, indicating a better fit. An oxygen-rich model with or without a thermal inversion also provides a worse fit to the data compared to the carbon-rich model. Consequently, the present data favour the interpretation of a carbon-rich atmosphere with no thermal inversion in WASP-12b.

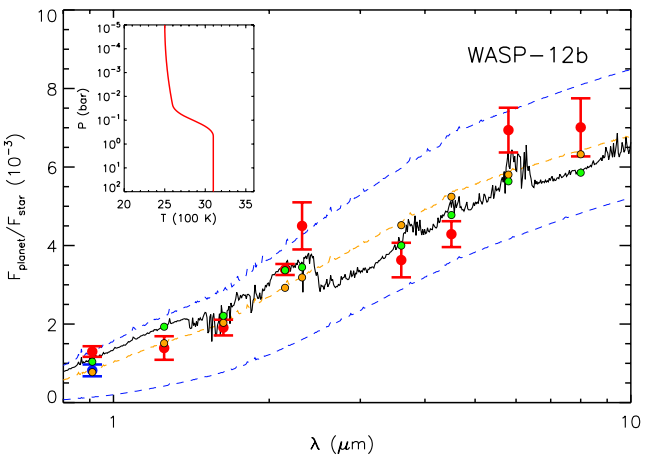

Figure 4. Observations and model secondary eclipse spectrum of WASP-12b. Our z'-band eclipse depth is shown as the red filled circle with error bars at 0.91 μm, together with previously published photometric observations at other wavelengths reported by Croll et al. (2011), Campo et al. (2011), Cowan et al. (2012) and Crossfield et al. (2012). The blue circle with error bars beneath our data shows the previously published data in the z' band by López-Morales et al. (2010) (see Section 5). The black solid curve represents a best-fitting model emission spectrum of the dayside atmosphere of WASP-12b with a carbon-rich composition and no thermal inversion. The orange dashed curve shows the best-fitting blackbody model with a temperature of 3135 K. The green circles without error bars represent the carbon-rich model integrated over the bandpasses of the data, while the orange circles are the integrated points for the blackbody model. The temperature profile is shown in the inset. The blue dashed curves denote two blackbody spectra with temperatures of 2200 and 3200 K shown for reference. The current data are best fitted by a carbon-rich model without a strong thermal inversion, consistent with the findings of Madhusudhan et al. (2011).

A more detailed atmospheric retrieval analysis and new data, which are beyond the scope of the current work, would be required to place tighter constraints on the C/O ratio of WASP-12b. In particular, we have used the *Spitzer* IRAC 3.6 and 4.5 μm flux contrasts reported by Cowan et al. (2012) and our present observation in the z' band. In doing so, a few other combinations of previous data sets at the same wavelengths have not been considered here. For example, considering the *Spitzer* IRAC 3.6 and 4.5 μm data from Campo et al. (2011), which have lower uncertainties, would make the carbon-rich model more likely and the isothermal model even less likely. On the other hand, we have used only one of the two values for the IRAC 4.5 μm point reported by Cowan et al. (2012) that is consistent with the value of Campo et al. (2011). Considering the alternate point could improve the fit for the isothermal model. Yet other combinations result from using the previously reported z'-band flux of López-Morales et al. (2010) instead of our current observation in the same band. We also note that a high-confidence narrow-band photometric observation at 2.3 μm might be able to provide a good constraint on the CO abundance. Future observations at this wavelength with more out-of-eclipse data than reported in Crossfield et al. (2012) could provide a longer temporal baseline for a reliable estimate of the eclipse depth. We have also not used the thermal spectrum of WASP-12b obtained in the *Hubble Space Telescope* Wide Field Camera 3 bandpass (1.1–1.6 μm), reported by Swain et al. (2013), as it has not yet been corrected for contamination due to the stellar companion (Crossfield et al. 2012). A detailed atmospheric retrieval analysis of WASP-12b based on the various combinations of these existing, and possibly re-reduced and/or corrected, data sets will be pursued in a future study.

6 DISCUSSION

Our observed eclipse depth, i.e. the planet–star flux ratio, in the z' band is 58 per cent higher than that reported by López-Morales et al. (2010). This disagreement is at the 2.4σ level and there are examples in the literature suggesting that this is not uncommon, e.g. the z'-band measurements of WASP-19b by Burton et al. (2012) and Lendl et al. (2013). If this difference is of physical origin, as opposed to a systematic error, it may be evidence for temporal variability in the stellar or planetary flux. In principle, stellar variability may be caused due to stellar flares, as suggested in Haswell et al. (2012), although this is unlikely given the spectral type of the host star. On the other hand, if the variability is in the emission from the planet, it would imply temporal changes in the temperature distribution on the dayside hemisphere of WASP-12b at pressures close to the planetary photosphere in the z' band, typically around 1 bar.

Assuming that the stellar flux in the z' band is constant, our observation implies a 58 per cent increase in the hemispherically averaged dayside thermal emission from WASP-12b over that observed by López-Morales et al. (2010). Since the two observations were separated in time by two months, it may be possible that transient effects due to atmospheric dynamics might be causing

the observed differences. Indeed, some general circulation models (GCMs) of hot Jupiters predict that large enough spatial structures, e.g. circumpolar vortices, in their atmospheres could cause temporal photometric variations in thermal emission from their dayside atmospheres (e.g. Rauscher et al. 2007; Cho et al. 2008; but cf. Showman et al. 2009). Rauscher et al. (2007) explored possible photometric variability in several hot Jupiters as a function of their mean zonal wind speeds and radiative forcing. For the example of hot Jupiter HD 209458b, their models showed variations as high as 60–70 per cent for wind speeds of 800 m s^{-1}. While a similar calculation has not been reported in the literature for WASP-12b, the order of magnitude higher incident irradiation received by WASP-12b compared to HD 209458b would imply higher wind speeds in WASP-12b and might cause the observed variability. GCM models of WASP-12b in the future would be able to investigate this possibility. Recent work by Fossati et al. (2013) has shown that variability of a G-type star due to star spots would cause a magnitude variation of ∼0.2 per cent. This amount is too low to explain our variable eclipse depth. Other work by Henry et al. (2013) has found absorbing gas around WASP-12. A variable cloud of gas might cause some Rayleigh scattering, but that would be significant mainly in the visible, and not much in the red–optical where our z' band lies. The effect of a steady-state circumstellar disc or cloud of gas should cancel out when we subtract the in-eclipse and out-of-eclipse fluxes to obtain the eclipse depth.

We have also explored the possibility of local variations in the surface brightness of the dayside atmosphere of WASP-12b caused due to potential transient effects, e.g. 'storms', following Agol et al. (2010). We considered a two-component z'-band brightness temperature distribution of the dayside hemisphere of the planet – a homogeneous background temperature (T_0) and a local perturbation with a temperature $T_1 = T_0 + \Delta T$ over a region with a parametric covering fraction (f), i.e. the fraction of the surface area covered by the perturbation. Assuming nominal covering fractions of $f = 0.1$–0.2 (Showman et al. 2009; Agol et al. 2010), we find that the difference between the two observed z'-band fluxes can be caused by temperature fluctuations of ∼450–750 K or higher, relative to a background temperature of ∼3000 K.

7 CONCLUSIONS

We have detected emission from WASP-12b in the z' band. We measure the eclipse depth at 0.91 μm to be 0.130 ± 0.013 per cent, significantly deeper in comparison to previous data. Assuming that this difference is not caused by systematics, and that the stellar flux is unchanging given the early spectral type of the star, the observed discrepancy may be caused by a temporally variable photospheric temperature of the planet. Local thermal fluctuations in the surface brightness distribution of the planet caused by atmospheric dynamics may be able to explain the observed variability, which can be further constrained using GCMs of WASP-12b in the future. Considering our z'-band observation along with previously reported photometric observations in other bandpasses, we find that the sum total of data are best explained by a carbon-rich model, with no evidence for a strong thermal inversion, as has been previously reported. We also estimate the mid-eclipse phase of the planet to be 0.501 ± 0.002, which corresponds to a circular orbit.

ACKNOWLEDGEMENTS

DF, VSD, TRM, SPL, CMC and ULTRACAM are supported by the STFC. This work is based on observations obtained with the 4.2 m William Herschel Telescope operated on the island of La Palma by the Isaac Newton Group in the Spanish Observatorio del Roque de los Muchachos of the Instituto de Astrofsica de Canarias. NM acknowledges support from the Yale Center for Astronomy and Astrophysics (YCAA) through the YCAA postdoctoral prize fellowship at Yale University.

REFERENCES

Agol E., Cowan N. B., Knutson H. A., Deming D., Steffen J. H., Henry G. W., Charbonneau D., 2010, ApJ, 721, 1861
Batygin K., Stevenson D. J., 2010, ApJ, 714, L238
Bergfors C., Brandner W., Henning T., Daemgen S., 2011, in Sozzetti A., Lattanzi M. G., Boss A. P., eds, Proc. IAU Symp. 276, The Astrophysics of Planetary Systems: Formation, Structure, and Dynamical Evolution. Cambridge Univ. Press, Cambridge, p. 397
Bergfors C. et al., 2013, MNRAS, 428, 182
Bodenheimer P., Laughlin G., Lin D. N. C., 2003, ApJ, 592, 555
Burton J. R., Watson C. A., Littlefair S. P., Dhillon V. S., Gibson N. P., Marsh T. R., Pollacco D., 2012, ApJS, 201, 36
Campo C. J. et al., 2011, ApJ, 727, 125
Chan T., Ingemyr M., Winn J. N., Holman M. J., Sanchis-Ojeda R., Esquerdo G., Everett M., 2011, AJ, 141, 179
Charbonneau D. et al., 2005, ApJ, 626, 523
Cho J. Y.-K., Menou K., Hansen B. M. S., Seager S., 2008, ApJ, 675, 817
Cowan N. B., Machalek P., Croll B., Shekhtman L. M., Burrows A., Deming D., Greene T., Hora J. L., 2012, ApJ, 747, 82
Croll B., Lafreniere D., Albert L., Jayawardhana R., Fortney J. J., Murray N., 2011, AJ, 141, 30
Crossfield I. J. M., Barman T., Hansen B. M. S., Tanaka I., Kodama T., 2012, ApJ, 760, 140
de Mooij E. J. W., Snellen I. A. G., 2009, A&A, 493, L35
Deming D., Seager S., Richardson L. J., Harrington J., 2005, Nat, 434, 740
Deming D., Harrington J., Seager S., Richardson L. J., 2006, ApJ, 644, 560
Dhillon V. S. et al., 2007, MNRAS, 378, 825
Enoch B., Collier Cameron A., Horne K., 2012, A&A, 540, A99
Fossati L., Ayres T. R., Haswell C. A., Bohlender D., Kochukhov O., Flöer L., 2013, ApJ, 766, L20
Gillon M. et al., 2009, A&A, 496, 259
Haswell C. et al., 2012, ApJ, 760, 79
Hebb L. et al., 2009, ApJ, 693, 1920
Henry G. W. et al., 2013, ApJ, 768, 155
Huang X., Cumming A., 2012, ApJ, 757, 47
Husnoo N. et al., 2011, MNRAS, 413, 2500
Ibgui L., Burrows A., Spiegel D. S., 2010, ApJ, 713, 751
Kiefer J., 1935, Proc. Am. Math. Soc., 4, 502
Lendl M., Gillon M., Queloz D., Alonso R., Fumel A., Jehin E., Naef D., 2013, A&A, 552, A2
Li S.-L., Miller N., Lin D. N. C., Fortney J. J., 2010, Nat, 463, 1054
Llama J., Wood K., Jardine M., Vidotto A. A., Helling C., Fossati L., Haswell C. A., 2011, MNRAS, 416, L41
López-Morales M., Seager S., 2007, ApJ, 667, L191
López-Morales M., Coughlin J. L., Sing D. K., Burrows A., Apai D., Rogers J. C., Spiegel D. S., Adams E. R., 2010, ApJ, 716, L36
Madhusudhan N., 2012, ApJ, 758, 36
Madhusudhan N., Seager S., 2009, ApJ, 707, 24
Madhusudhan N. et al., 2011, Nat, 469, 64
Moffat A. F. J., 1969, A&A, 3, 455
Perna R., Heng K., Pont F., 2012, ApJ, 751, 59
Pont F., Zucker S., Queloz D., 2006, MNRAS, 373, 231
Press W., Teukolsky S., Vetterling W., Flannery B., 2007, Numerical Recipes, 3rd edn: The Art of Scientific Computing. Cambridge Univ. Press, Cambridge
Rauscher E., Menou K., Cho J. Y.-K., Seager S., Hansen B. M. S., 2007, ApJ, 662, L115
Rogers J. C., Apai D., López-Morales M., Sing D. K., Burrows A., 2009, ApJ, 707, 1707

Sackett P. D., 1999, in Mariotti J.-M., Alloin D., eds, NATO ASIC Proc. Vol. 532, Planets Outside the Solar System: Theory and Observations. Kluwer, Dordrecht, p. 189
Schwarz G., 1978, Ann. Stat., 6, 461
Showman A. P., Fortney J. J., Lian Y., Marley M. S., Freedman R. S., Knutson H. A., Charbonneau D., 2009, ApJ, 699, 564
Sing D. K., López-Morales M., 2009, A&A, 493, L31
Southworth J. et al., 2009, MNRAS, 396, 1023
Swain M. et al., 2013, Icarus, 225, 432
Zhao M., Monnier J. D., Swain M. R., Barman T., Hinkley S., 2012, ApJ, 744, 122

This paper has been typeset from a TEX/LATEX file prepared by the author.